Experimental analysis of high and steep wave impacts and related hydroelastic effects relevant for offshore structures in steel

Ahani, A.[1,*] Abrahamsen, B.C.[2], and Greco, M.[3]

[1] Department of Marine Technology, NTNU, Trondheim, Norway (alireza.ahani@ntnu.no)
[2] SINTEF Ocean, Trondheim, Norway (bjornchristian.abrahamsen@sintef.no)
[3] Department of Marine Technology, NTNU, Trondheim, Norway/CNR-INM, Institute of Marine Engineering, Rome, Italy (marilena.greco@ntnu.no/marilena.greco@cnr.it)

Abstract. An experimental strategy to investigate high and steep wave impacts and related hydroelastic effects relevant for offshore structures in steel is proposed. A physical model was shaped as a vertical rectangular surface-piercing column mimicking a semi-submersible leg at the scale of 1:40 and studied in irregular waves with two different setups, respectively, a rectangular A) rigid and a B) flexible panel installed in the impact zone. The measurements at discrete locations of the rigid and flexible panels are pressure and strain, respectively, synchronized with wave measurements and high-speed videos. The steps of the analysis involve preliminary hammer tests in dry flexible panel and the wave tests with setup A) and B) and their comparative analysis so to identify the features of the critical wave-impact scenarios, and those of the excited modes and involved added-mass effects. These steps are described using one of the most critical wave-impact scenarios observed in the tests.

Key words: *Experiments; steep waves; impact scenario; semi-submersible leg; hydroelastic effects*

1. Introduction

High breaking waves are known to be of great danger in local/global integrity of offshore structures as consequence of slamming events. Present work is part of an ongoing research activity, which focuses on local structural response within the industrial project SLADE KPN. In fact the severe effect of wave slamming could cause immediate damages to the local structure exposed to the wave; in this regard, it is crucial to identify the physics relevant for the structure's response. The purpose of the current study is to investigate wave-impact scenarios in a physical lab to identify and analyse the critical events in terms of hydrodynamic exciting effect (local incident waves) and corresponding response (measured pressure and strain), and to characterize the importance of hydroelastic effects. The results are useful to improve standards and design guidelines for offshore structures. In this context, the proposed research strategy consists of 1) a preliminary modal analysis of the structure through dry impact tests and FEM analysis, to identify dry modes and related natural periods, 2) detect the most severe wave-impact scenarios observed in tests and, for that, 3) examine the excitation loads induced on the rigid panel (setup A) and the structural response of the flexible panel (setup B) in time and in frequency (with FFT and wavelet transform of the signals) domain analyses. We present the experimental set-up, preliminary impact tests for dry-modes identification, and the proposed analysis strategy applied to one of the critical wave-impact scenarios identified in the tests. Then conclusions and further research steps are outlined.

---

*Correspondence to: alireza.ahani@ntnu.no

2. Experimental Setup

A systematic experimental study of wave impact was carried out in the towing tank at SINTEF Ocean. A rectangular vertical cylindrical model was attached to the carriage, fixed in all degrees of freedom (see a photo of the setup in Fig.1) and placed in the tank so that it interacted with steep and nearly breaking waves. The structure mimics a semi-submersible leg at the scale of 1:40. In the following, all

Figure 1: Experimental setup: the rectangular cylinder with flexible panel installed against the wave-maker. The structure is mounted on the carriage bridge.

quantities are given in model scale unless explicitly stated. In the first series of tests, irregular and focused waves were calibrated in the setup without presence of structure (see part A in Fig.2). At the next stage, the same waves were generated in presence of the structure (see part B in Fig.2). The structure is located 34.5 m distant from the wave-maker with neighbouring wave probes detailed in the Fig.2. The wave probes RW1-RW8 were used to monitor the local incident wave. The vertical (C) and transverse (D) views of the structure with corresponding details are presented in Fig.2. The used wave probes have an expected error of few millimeters, the frame rate of the cameras is 3.03 kHz. The measurements at discrete locations of the rigid and flexible panels are pressure and strain, respectively, synchronized with wave measurements and high-speed videos. Both panels cover the same surface area exposed to waves (see Fig.3). Considering the flexible panel, the full scale material is steel with Young's modulus of 210 GPa and Poisson ratio $\nu = 0.3$, and the 3D printed model is made of a viscoelastic material with approximate linear Young's modulus of 2.7 GPa, $\nu = 0.39$ and density of $1170 kg/m^3$. Sketches of the flexible and rigid panels are documented in Fig.3. In the rigid case, an equivalent force is estimated by integrating the measured pressure over the sensor surface and from now on is called force measurement.

3. The Analysis

The research steps carried out within the proposed strategy are presented next.

3.1. Processing tools for the analysis

The signals measured by the pressure and strain gauges were preliminary denoised so to avoid unphysical high frequency content; the approach used is the one documented in a similar study on wave slamming [1] with more details in [2]. Then, a time-frequency representation of the signals, in the form of a continuous wavelet transform (WT), has been implemented. This allows to document the change in
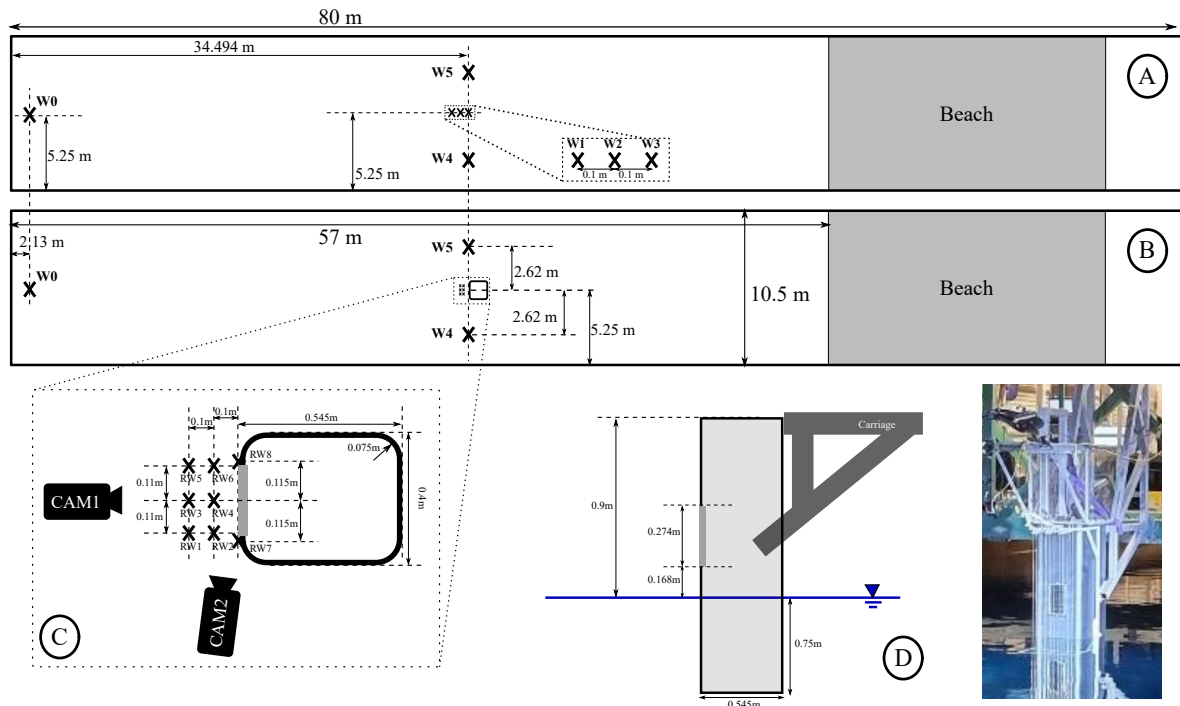
Figure 2: Sketch of experimental setup without (A) and with (B) the structure (top view). C: sketch of the structure and camera system used for the video recordings (top view). D: side-view sketch of the structure and picture from the physical tests. The main dimensions are specified. The wave probe positions are shown by ×.

time of the frequency content in non-stationary signals. The implemented wavelet function is a two parameter analytic Morse wavelet [3], which preserves an accurate amplitude of the frequency components in the signal [4]. The frequency content of the WT output is over a certain range of discrete frequencies, identified by following the procedure in [5].

3.2. Natural frequencies of the dry panel

After bolting the flexible panel to the structure and installing the cylinder as depicted in part D of Fig.2, a set of impact tests has been carried out. First, hammer tests were carried out. It was found that the heavy hammer impact causes a significant inertia effect on the panel, which makes the assumption of free-vibration very rough, therefore more difficult to identify the dry natural frequencies. Therefore another object (a pencil) was chosen to impact the panel with. The identified first natural frequency by Fourier transform appeared to be very similar in both cases (2% difference). We have also checked another flexible panel (not detailed here), and the natural frequencies were completely different from those of the panel examined here (35% difference); this indicates that we can disregard contribution of the flexibility of the surrounding structure into the panel features. The strain gauge response measured by in the pencil tests as a result of impact at the points F1-F5 (see Fig.3) is studied with Fourier Transform and wavelet transform. The imaginary part of the complex WT allows to monitor the time evolution of the frequency content in the signal while the FFT provides the average frequency content. Exemplifying results are documented in Fig.4, confirming a good agreement between the two independent results. As complement to the physical investigation, we built a finite element model (FEM) of the panel with hexahedral fully integrated elements to estimate the mode shapes and related dry natural frequencies. The element spatial discretization size is approximately 1mm. The first 10 modes were identified and the first four of them are demonstrated in Fig.5. The applied boundary condition on the FEM of the
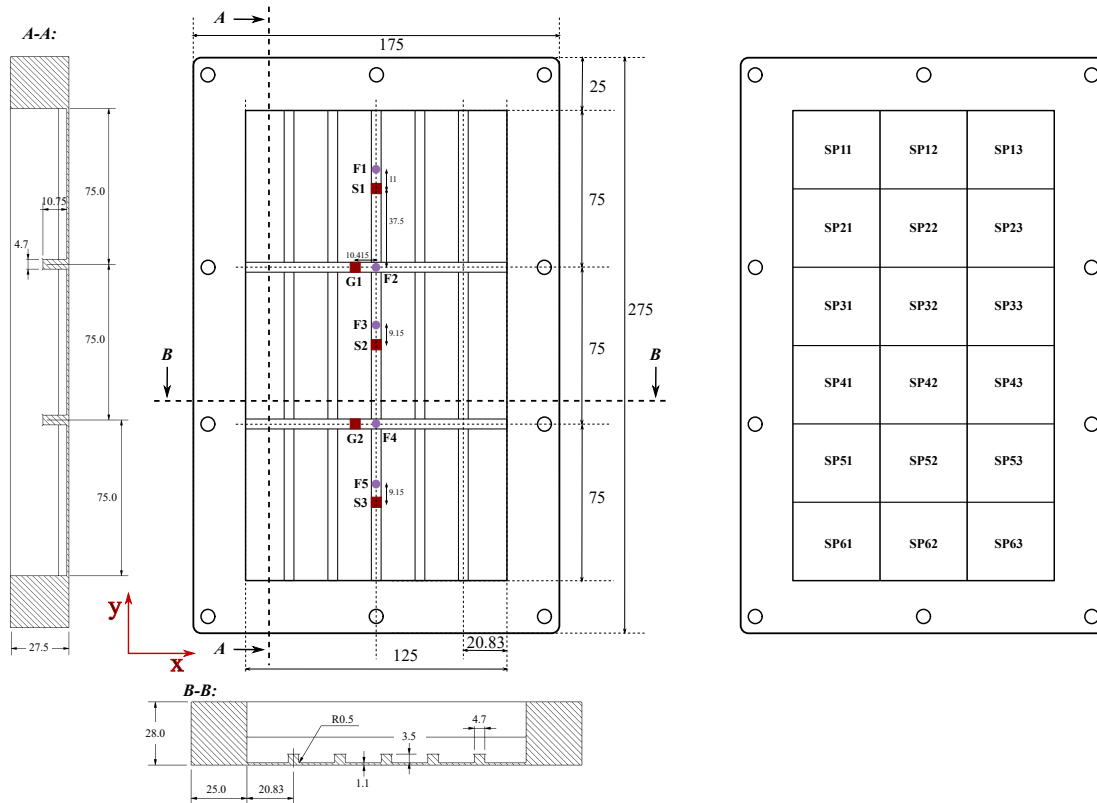
Figure 3: Panel dimensions for the flexible (left) and rigid (right) panel. The vertical and horizontal sections of the flexible panel are also specified in this figure. The F points represent impact test locations, the S and G specify the positions of the strain gauges on stiffeners and girders, respectively. There are strain gauges at the same locations both outside (external or wet side) and inside (internal or dry side) the cylindrical structure. The SP represents slamming panels for measuring the pressure.

panel is fixed nodes within the bolt holes; the influence of boundary conditions on the plate features will be examined in a next research step. Based on the identified mode shapes in Fig.5, we can establish a relationship between the dry test impact locations (F1-F5) and the possible excited modes because, if we hit a modal node, there would be a zero excitation of that mode in theory. This is shown in Fig.4 where for example there is no excitation in mode 1 due to impact in F1. The figure also includes imaginary part of the WT to show phase difference between different frequency components over time. The impact with pencil object at location F5 excites two modes with frequencies 550 and 715 [Hz] (see the FFT at G1), they are also pronounced in the corresponding WT, also reported in the figure. For both transforms the amplitude of the component with frequency 715 [Hz] is almost twice that of the component with frequency 550 [Hz] after t=0.009 [s]. A similar consistency between FFT and WT results can be observed for impact at F4. Using this analysis, we can identify the dry modes that the different pencil impacts can excite on the flexible panel; they are documented in Table 1. In Fig.4, the solid black lines indicate eigen-frequencies of the panel identified by the FEM. They appear slightly higher than the corresponding frequencies extracted from the free-vibration phase of the strains in the impact test. The discrepancy could be due to the fact that the panel is mounted on a column partly inside water (see Fig.2-D), but other checks will be examined to identify its main reason.

3.3. Incident irregular waves

Here, we examine the irregular waves generated in the tests. They simulate high and steep waves occurring in North-Sea storm conditions with 100-years return period. The theoretical waves correspond
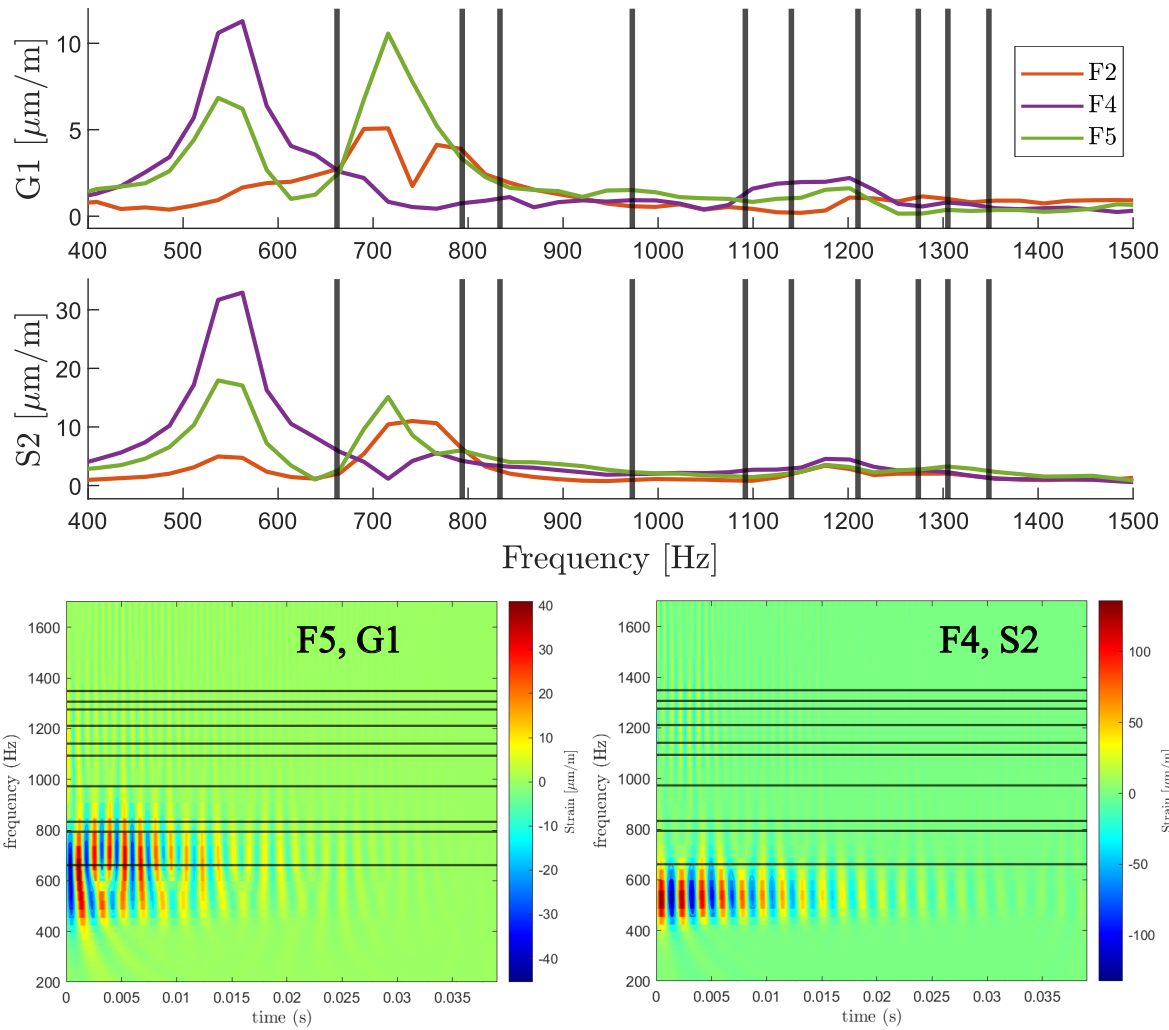
Figure 4: The frequency content of the panel strain response identified from pencil impact in dry condition. Top: FFT of the strain in G1 and S2 due to impact in F2, F4 and F5. Bottom: Imaginary part of the gauge strain WT (Fj, Sk: indicates impact at Fj and measurement at Sk).

to a long-crested system related to a JONSWAP spectrum with significant wave height of $13.3\ m$, peak period of $13.7\ s$ and peak-enhancement factor $\gamma = 3.0$ (see the formula in [6]), and the corresponding quantities are scaled down to 1:40 for holding the similarity. The duration of each wave generation was set to 20 minutes. The repeatability of the waves generated with different seeding is analysed in terms of their amplitude spectra, which are also compared with the theoretical JONSWAP spectrum in Fig.6. The implemented method of experimental spectrum estimation is the modified periodogram estimation (MPE) or Welch's method, in this method the hamming windows have 50% overlap. The estimated spectra are averaged over 18 different seeded waves. The results confirm a satisfactory repeatability and reliability of the incident waves when there is no structure. The presence of the structure leads to an increased energy in the spectrum at frequencies near to and higher than the peak theoretical frequency due to more pronounced reflection of shorter wave components from the structure. This is documented by the close and upstream probe RW4 while less effect is shown by the side probes WP4 an WP5, confirming a local wave steepening in front of the structure.

(a) 1st mode (f=662 [HZ]).

(b) 2nd mode (f=794 [HZ]).

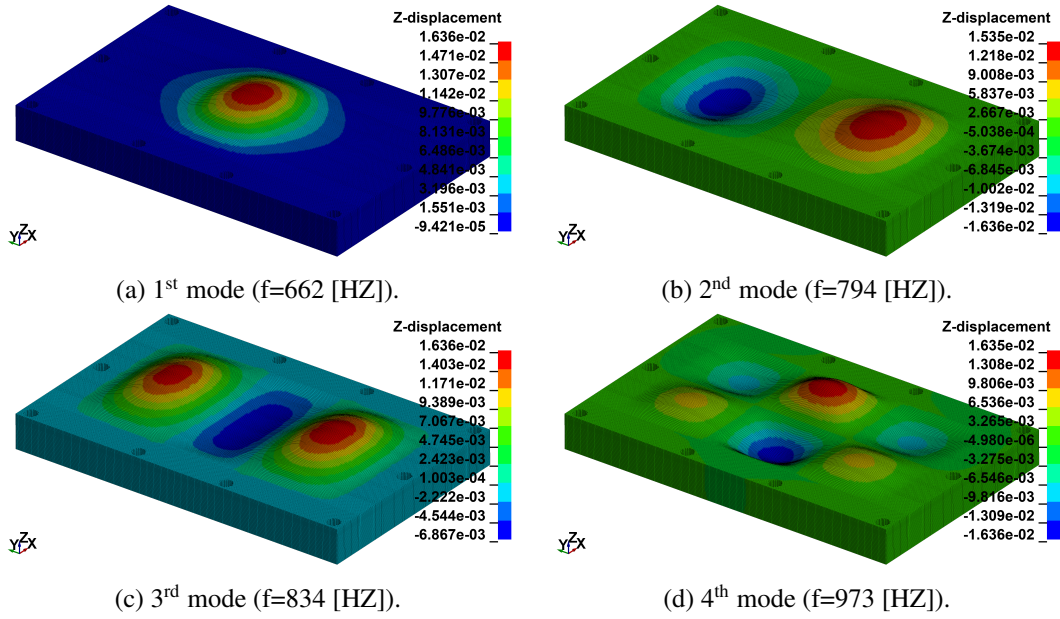(c) 3rd mode (f=834 [HZ]).

(d) 4th mode (f=973 [HZ]).

Figure 5: The first four eigenmodes from the FEM solution shown as Z displacement.

Table 1: Dry impact locations and corresponding excited modes from approximate FEM solution

Impact point	Node ID in FEM	relevant modes
$F1$	48074	2nd, 3rd, 7th, 9th, 10th
$F2$	49582	1st, 2nd, 3rd
$F3$	52696	1st, 3rd, 7th, 10th
$F4$	49870	1st, 2nd, 3rd
$F5$	56548	2nd, 3rd, 7th, 8th, 9th, 10th

3.4. Selected wave-impact case

From a preliminary screening of the wave-impact cases, the most critical events were identified and one of them selected as test case for the analysis. [h] Its related wave elevation time series at probe W2 is depicted in Fig.7 and the snapshots of the impact, which occurs within the highlighted interval of Fig.7, are demonstrated in Fig.8. The primary steps of the proposed analysis strategy are applied in the following to this selected case and represent an ongoing research. Based on the videos, see Fig.8, the selected wave-impact case corresponds to a a steep wave with a sharp profile and developing into a plunging phase when it hits the structure. This breaking wave introduces an air pocket near the panel, as can be seen in t=376 ms of the figure, and induces on the rigid panel the total excitation force shown in Fig.9. In the left of the figure, it is also provided the corresponding wave elevation at probe RW2. This wave probe is 0.1 m upstream of the panel (see C in Fig.2), so it gives a good impression of the wave evolution up to a certain phase of the slamming. The features of the incident waves appear very similar in the flexible panel setup (see B in Fig.2) and indicate indirectly a steep local wave due to the fast rise up. We observe a time shift of about 0.08 s between the wave elevations; this should be considered to synchronize the slamming force (from set-up A) with the strain measurements (from set-up B). The rise-up time of the measured force on the rigid panel (Fig.9) is quite short compared with the first dry natural period, therefore it is expected that the flexible panel experienced free vibrations in this wave-impact
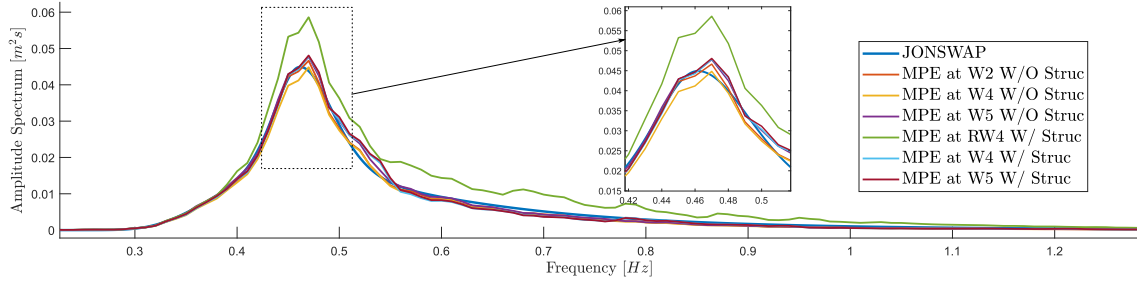
Figure 6: Wave amplitude spectrum: the theoretical JONSWAP spectrum is compared with the averaged spectra of 18 generated waves (with different seeding).
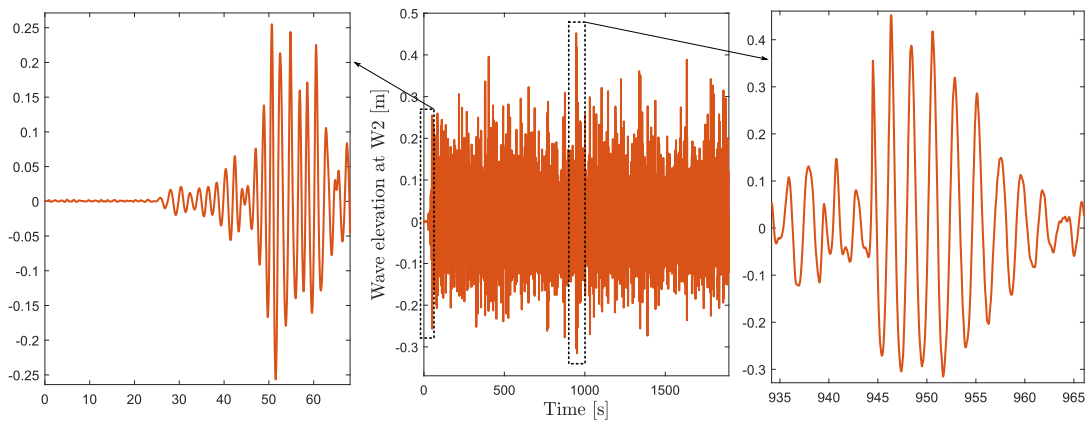

Figure 7: Time series of the generated wave at W2 in the experiment without structure (see the A in figure 2); the initial phase of wave generation and the slamming phase are highlighted.

case because added-mass effects will tend to increase even further the natural period.

With the previously discussed parts, we can now implement a similar strategy to examine the hydro-elastic response in terms of structural modes. First of all, we need to have an impression of the exciting force, this is provided by the slamming force measured on the rigid panel documented in right side of Fig.9 in terms of time and frequency (through WT) evolution. The force shows a quick rise-up connected to the initial impact and then an oscillatory behavior at frequency about 171 Hz lasting for about $0.04s$ after the initial impact. The latter is reasonably connected with the air-cavity entrapment and so to the related natural frequency. Figure 10 shows the magnitude of the wavelet transform of the strain at the internal and external gauges in G2, together with their time signals. The vertical lines in the plots of the figure specify the same time instants of the process. These results indicate an initial dominating frequency slightly higher than that in the force measurements (i.e. about 197 Hz) but with similar duration. This suggests that such oscillation frequency is also connected with air-cavity entrapment but in the present case the initial volume of the cavity must be slightly smaller. The strain measurements also indicate a lower frequency (about 113 Hz) that lasts also after the air-cushion phenomenon is over. The latter is reasonably connected with the natural frequency of the flexible panel in the wave-impact condition. Comparing this with the lowest oscillation frequency identified in the pencil experiments (i.e. about 550 Hz), we clearly identify an important reduction possibly due to added-mass effects. If we apply a 1DOF mass-spring model to the first structural mode and assume that in the two scenarios (pencil test and wave-impact test) the spring effect is unchanged, then we should have a generalized added mass-to-mass ratio about 23. This seems to be quite high, but a ratio of similar magnitude is observed connected with theoretical and experimental studies of wave impact on horizontal elastic plates in steel, as documented e.g. in [7]. Because the material used for the flexible panel is viscoelastic, one
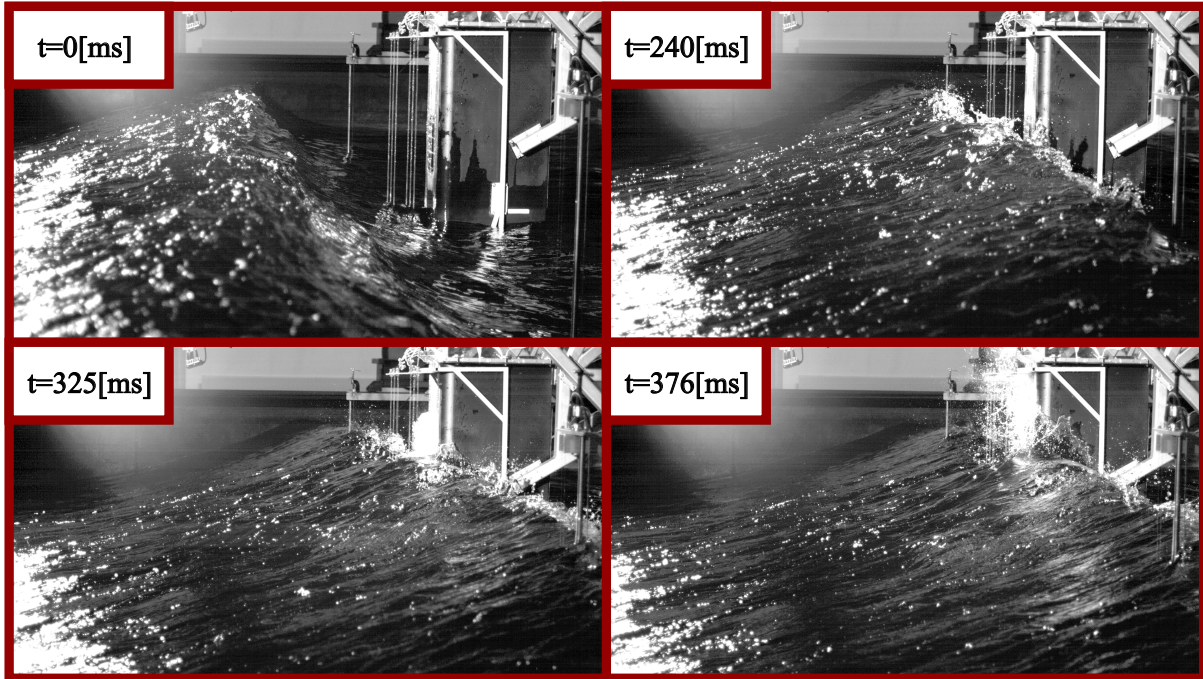
Figure 8: Snapshots of the selected wave slamming event. The wave approaches the panel from left to right. The time instants of the snapshots are not synchronized with the plots.

should assess possible changes in the spring effects. Besides this, an important next research step will be to analyse the features of the wetting during impact and combine the physical analysis with simplified estimates of the added-mass effects for different wetting conditions.

Table 2 provides the amplitude of the first mode of the panel as estimated from the free-vibration stage of the strain signals for the examined wave-impact case; the corresponding values from the G2-out and G2-in (see Fig.10) can also be found in this table. Figure 11 compares the strain amplitudes associ-

Table 2: The identified first wet mode amplitude from strain gauge

Strain Gauge	S1-out	G1-out	S2-out	G2-out	S3-out	S1-in	G1-in	S2-in	G2-in	S3-in
Amp $[\mu\frac{m}{m}]$	116	247	315	280	167	119	441	529	441	204

ated with this first mode for the panel in wave-impact scenario with that of the panel in dry conditions, i.e. identified from the pencil impact case at F3. They were obtained using FFT. The abscissa indicates the strain gauges on both sides of the panel (see Fig.3) and the strain amplitudes are normalized with the corresponding amplitude at the S2-in value for this mode. The left half of the plot belongs to the external sensors (out) and the other half to the corresponding values from the internal strain gauges (in). Consistently with the experimental setup, the gauges on stiffeners provide the principal strain along the length of the panel (ϵ_{yy}), and the gauges on the girders provide the same value along the width of the panel (ϵ_{xx}). On the internal side of the panel, the gauges measure higher strains due to the larger distance of this location from the neutral axis of an equivalent beam. Though the strain amplitudes measured refer to different directions (x or y) depending on the gauges, their values have been connected to highlight
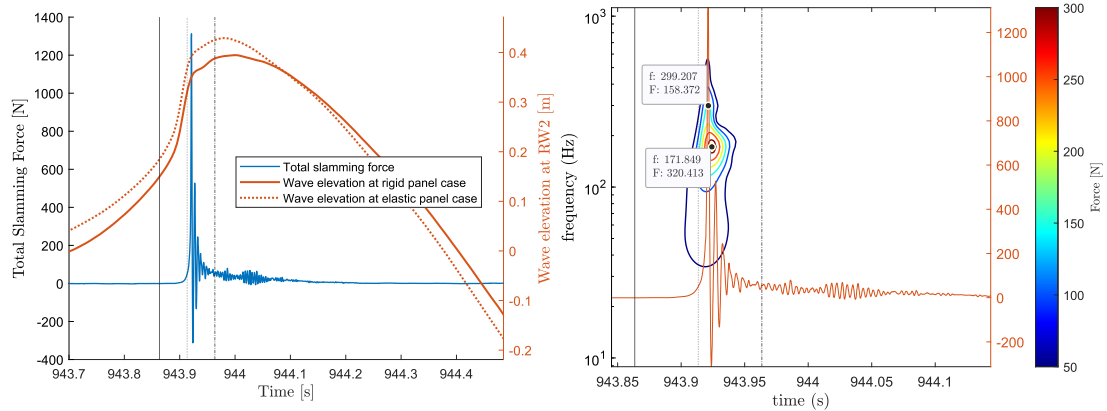
Figure 9: Left: Total force measurement on panel as result of the selected wave-impact case together with the wave elevation measured at RW2. The vertical lines correspond to the time instants highlighted in the strain gauge analysis (e.g. Fig.10). Right: WT of the Force.
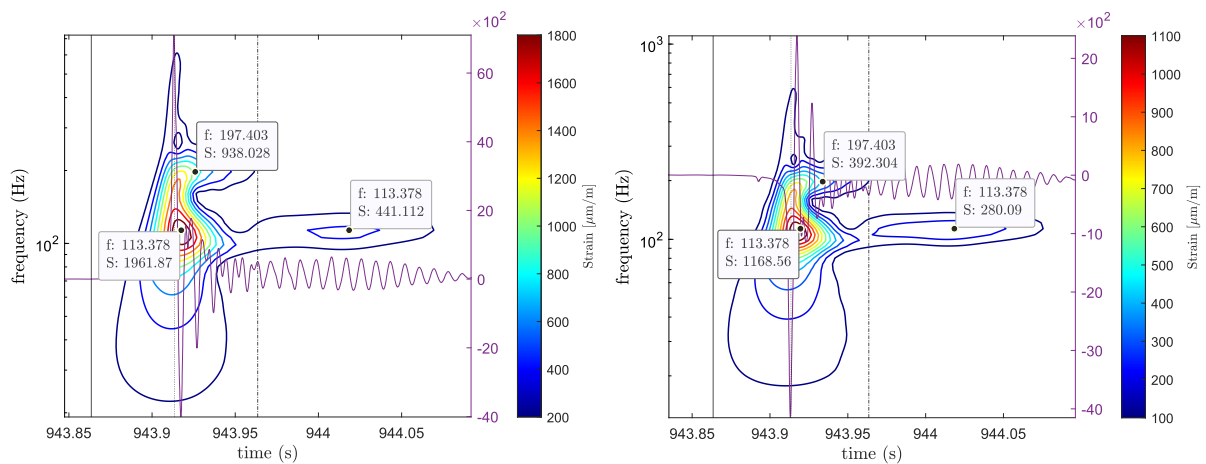

Figure 10: Strain gauge measurement signal and WT at G2 (Left: dry side (in), Right: wet side (out)).

the behavior shown for the first mode in the dry and in the wave-impact scenarios, and compare them. The results confirm similar shapes in the two panel conditions. They also indicate that the symmetry properties of the first mode, as identified by the FEM, are not fully satisfied; this requires further study and is part of our ongoing research.

4.   Conclusions

In this study the hydro-elastic problem of severe wave-structure interaction was studied experimentally and complemented by a FEM modal analysis. As an address to ultimate loading state design of the wave impact to the structure we selected one of the most severe wave impacts documented in the experiments as test case of the proposed analysis strategy. The corresponding breaking wave was modeled by generating North sea 100-year irregular waves and it interacted with a vertical cylindrical structure mimicking a semi-submersible leg, with an installed rigid or flexible panel in the impact zone. The automatic camera recording indicated that the event is a plunging breaker. The frequency domain analyses (using FFT and WT) of the slamming force and strains, respectively, on the rigid and flexible panels, combined with the FEM results, gave us an impression of the dry and wet modes of the response, allowed us to identify the occurrence of gas-cavity entrapment and to examine the effect of added mass in terms of the frequency and shape of the first mode. Further research steps include, among the others, a simplified
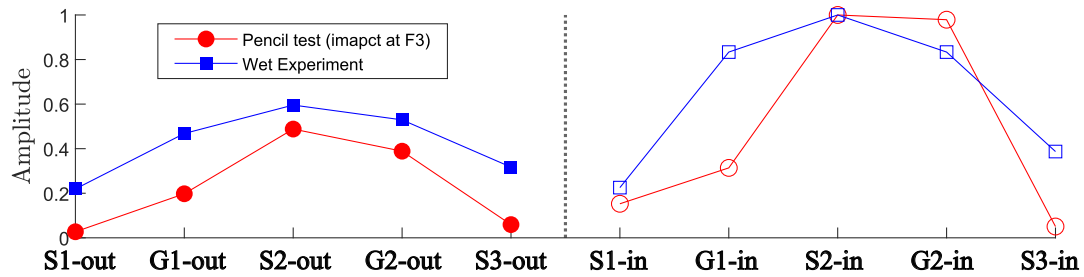
Figure 11: The normalized (with S2-in) first mode amplitude of the Wet slamming experiment obtained by WT, and dry mode FFT amplitude obtained by pencil impact at F3. Abscissa lists different strain gauges.

added-mass modeling and its assessment against the experiments, as well as a more in-depth use of the synchronised video recordings for a better physical understanding of the wetting phenomena.

5. Acknowledgement

References

[1] Y Guo, L. Xiao, X. Teng, Y. Kou, J. Liu, Processing method and governing parameters for horizontal wave impact loads on a semi-submersible. *Marine Structures*, 69, 2020, DOI: 10.1016/j.marstruc.2019.102673

[2] D. L. Donoho, De-noising by soft-thresholding. *IEEE Transactions on Information Theory*, 41(3): 613–627, 1995, DOI: 10.1109/18.382009

[3] S. C. Lilly, Olhede J. M., Generalized Morse Wavelets as a Superfamily of Analytic Wavelets. *IEEE Transactions on Signal Processing*, 60(11): 6036–6041, 2012, DOI: 10.1109/tsp.2012.2210890

[4] J. M. Lilly,, Element analysis: a wavelet-based method for analysing time-localized events in noisy time series. *Proceedings of the Royal Society A: Mathematical, Physical and Engineering Sciences*, 473 2017, DOI: 10.1098/rspa.2016.0776

[5] J. M. Lilly, Olhede, S. C., Higher-Order Properties of Analytic Wavelets. *IEEE Transactions on Signal Processing*, 57(1):146–160, 2009, DOI: 10.1109/tsp.2008.2007607

[6] N. D. P. Barltrop, A. J. Adams, *Dynamics of Fixed Marine Structures (Third Edition)*, 249–344, Butterworth-Heinemann, 1991, ISBN: 978-0-7506-1046-9

[7] O. M. Faltinsen, *Hydrodynamics of high-speed marine vehicles*, Cambridge university press, 2005, 292–296 ISBN: 0521845688